Noise-enabled precision measurements of a Duffing nanomechanical resonator

J. S. Aldridge and A. N. Cleland
Department of Physics, University of California at Santa Barbara, Santa Barbara, CA 93106
(Dated: February 2, 2008)

We report quantitative experimental measurements of the nonlinear response of a radiofrequency mechanical resonator, with very high quality factor, driven by a large swept-frequency force. We directly measure the noise-free transition dynamics between the two basins of attraction that appear in the nonlinear regime, and find good agreement with those predicted by the one-dimensional Duffing equation of motion. We then measure the response of the transition rates to controlled levels of white noise, and extract the activation energy from each basin. The measurements of the noise-induced transitions allow us to obtain precise values for the critical frequencies, the natural resonance frequency, and the cubic nonlinear parameter in the Duffing oscillator, with direct applications to high sensitivity parametric sensors based on these resonators.

Doubly-clamped mechanical resonators have recently been the subject of much attention, due to the ability to make very high frequency, high quality factor resonators, with applications in weak force and small mass detection, frequency stabilization, and possibly quantum computation[1,2,3,4,5,6,7,8,9,10,11,12,13]. The limit for parametric sensing is often set by the precision with which a resonator parameter, such as the mass, can be monitored, limited typically by measurement and intrinsic noise sources. Here we show how one can use the intrinsic nonlinear response of these resonators, and the addition of external broadband noise, to significantly improve the measurement precision of two such parameters, the resonance frequency and the cubic nonlinearity. This has direct implications for the ultimate sensitivity of such parametric sensors.

At large drive amplitudes, doubly-clamped resonators exhibit a bistable response quantitatively similar to that of the Duffing oscillator[14,15]. The motion in the fundamental mode of a doubly-clamped beam is thus well-approximated by the Duffing equation, which for a natural resonance frequency Ω_0 and quality factor Q, driven at frequency Ω, has the form

$$M\frac{d^2Y}{dt^2}+M\frac{\Omega_0}{Q}\frac{dY}{dt}+M\Omega_0^2Y+KY^3=\mathcal{B}\cos(\Omega t)+\mathcal{B}_{noise}(t), \tag{1}$$

where Y denotes the displacement amplitude of the midpoint of the beam, M denotes the mass of the beam, $\mathcal{B}$ the amplitude of the external driving force, and $\mathcal{B}_{noise}(t)$ the stochastic forcing function due to thermal and external noise[6,14,15]. This equation assumes that the beam oscillates in the mode with natural frequency Ω_0, that the displacement amplitude $Y(t)$ is the only relevant degree of freedom, and that the equation of motion includes only the third-order nonlinearity, with strength K.

The displacement $Y(t)$ in Eq. (1) can be written as

$$Y(t)=U_1(t)\cos(\Omega t)+U_2(t)\sin(\Omega t), \tag{2}$$

in terms of the two quadrature amplitudes $U_{1,2}(t)$. For a high Q system driven at frequency Ω near Ω_0, the slowly-varying envelope approximation can be used[14,16], where the functions $U_{1,2}(t)$ are replaced by their slowly varying averages, $u_{1,2}(t)$, respectively.

In the absence of noise, the average functions $u_{1,2}(t)$ satisfy the equations of motion

$$\left.\begin{aligned}\frac{d^2u_1}{dt^2} &= (\Omega^2-\Omega_0^2)u_1-\frac{3}{4}\frac{K}{M}u_1(u_1^2+u_2^2)\\ &- \frac{\Omega_0}{Q}\Omega u_2-\frac{\Omega_0}{Q}\frac{du_1}{dt}-2\Omega\frac{du_2}{dt}+\frac{\mathcal{B}}{M},\\ \frac{d^2u_2}{dt^2} &= (\Omega^2-\Omega_0^2)u_2-\frac{3}{4}\frac{K}{M}u_2(u_1^2+u_2^2)\\ &+ \frac{\Omega_0}{Q}\Omega u_1-\frac{\Omega_0}{Q}\frac{du_2}{dt}+2\Omega\frac{du_1}{dt}.\end{aligned}\right\} \tag{3}$$

The Duffing oscillator exhibits one stable state for small drive amplitudes $\mathcal{B}$, while above a critical amplitude $\mathcal{B}_c$ a bifurcation occurs, creating two stable basins of attraction. One basin corresponds to larger displacement amplitudes, and is stable for drive frequencies up to an upper critical frequency ν_U ($\nu=\Omega/2\pi$), determined by the drive amplitude $\mathcal{B}$. The other stable basin has smaller displacement amplitude, and is stable for frequencies down to a lower critical frequency ν_L, also determined by the drive amplitude. The stable attractors are found by setting all time derivatives in Eq. (3) to zero and solving for $u_{1,2}$, yielding three equilibrium points. Two of these equilibrium points are stable foci, and the third is a metastable separatrix.

A transition between the two basins occurs in the absence of noise when the energy barrier separating them is reduced to zero, by changing either the drive amplitude or the drive frequency. In the presence of noise, however, the Duffing oscillator will exhibit stochastic transitions between the two basins. For weak noise signals, the transitions occur only near the critical frequencies $\nu_{L,U}$, while as the noise power is increased, the separation between the upper and lower transition frequencies is effectively reduced.

Here we make detailed measurements of the nonlinear dynamics of a doubly-clamped beam, investigating both the dynamical motion and the change in the inter-basin transition rates due to broadband noise. Our experimental system comprises a pair of doubly-clamped beams of single-crystal aluminum nitride, with dimen-

sions $3 \times 0.2 \times 0.14$ μm^3, oriented perpendicular to one another and fabricated together on a chip of single-crystal Si. The fabrication technique is described elsewhere[17]. The chip was placed in the vacuum bore of an $B = 8$ T magnet at 4.2 K, with one beam (the active beam) oriented perpendicular to the field direction, the other (reference) beam parallel to the field. Magnetomotive actuation and displacement detection was used to drive the active beam[1], where the parallel orientation of the reference beam decouples it from the drive force (see Fig. 1). The active beam had a natural resonance frequency $\nu_0 = \Omega_0/2\pi = 92.9$ MHz, a quality factor $Q = 6750$, and a critical drive power for inducing the hysteretic bifurcation of -61 dBm. Using the beam resistance of 11 Ω, this corresponds to a critical drive force $\mathcal{B}_c = 580$ pN, and a midpoint displacement of 18 nm.

Measurements were made with a radiofrequency bridge[18], as shown in Fig. 1(a). The rf drive signal is split by a 180° phase splitter, with the two phases passed through separate stainless coaxial cables of similar construction. The 180° phase-shifted signal is connected to one end of the reference beam, and the 0° signal connected to one end of the active beam. The other ends of the two beams are connected to a third coaxial cable that returns to room-temperature electronics. The bridge can be balanced in both amplitude and phase over the range of frequencies used in this experiment, and is typically tuned so that the electrical signal is proportional to the displacement-induced electromotive force[1].

The signal measured in the experiment is the demodulated output of the bridge, giving the in-phase and out-of-phase quadrature signals $I(t)$ and $Q(t)$. These are proportional, to within a phase factor, to the average amplitudes $u_{1,2}(t)$[1,18]. In Fig. 1(b)-(d) we display the response of the active beam to a range of drive amplitudes, where the frequency is swept through the resonance for each drive amplitude; the hysteresis in the amplitude and phase response is in quantitative agreement with the response expected for a Duffing oscillator.

In Fig. 2 we compare the measured quadrature amplitudes to numerical solutions of Eq. (3). In Fig. 2(a) we show the calculated phase-space trajectories, and in (b) and (c) the experimentally measured trajectories. In Fig. 2(d) and (e) the time traces are shown for the switching transitions. The correspondence between the image in (a) and those measured in (b) and (c) is quite clear. It can be shown that as the drive frequency is varied, the stable points will follow a circle on the $u_{1,2}$ plane, even in the presence of the Duffing nonlinearity. These circles are evident in Fig. 1(d).

We now turn to a discussion of the noise-induced transitions between the stable foci. The problem of thermally-activated escape from a potential landscape with a single basin of attraction is a thoroughly studied problem[19]. The escape rate over a barrier of height E_B is given by $\Gamma = a(Q)\nu_0 \exp(-E_B/k_BT)$, determined predominantly by the Arrhenius factor and less so by the Q-dependent prefactor $a(Q)$. Our system differs from

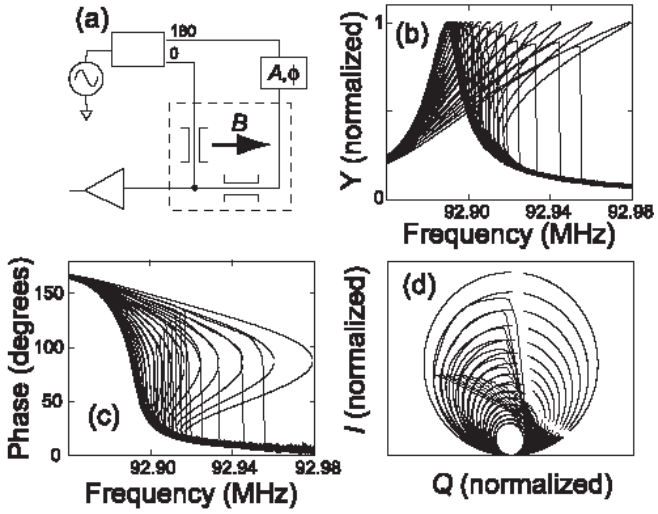

FIG. 1: (a) Schematic showing circuit and active and reference beams; dotted outline encloses cryogenic part of experiment. Box labelled $0, 180$ is a 180° phase splitter, and that labelled A, ϕ allows adjustment of the amplitude and phase of the signal. The arrow indicates the orientation of the magnetic field. (b) Hysteresis in amplitude versus drive frequency, for drive amplitudes from -68 to -53 dBm, in 1 dBm steps. (c) Hysteresis in phase for the same drive amplitudes as (b). (d) Hysteresis in $u_1 - u_2$ plane, plotted as I versus Q in dimensionless units.

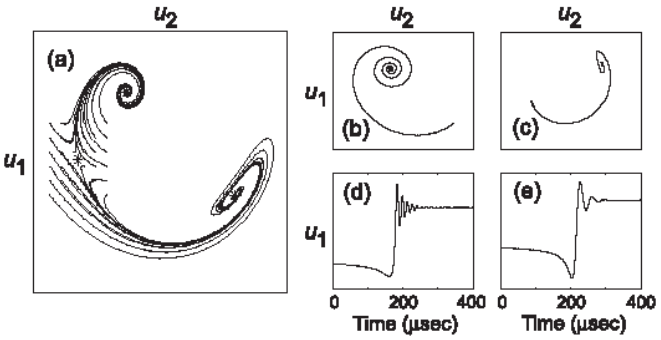

FIG. 2: (a) Numerically-generated phase-space flow for a drive force 9 dB above the critical point $\mathcal{B}_c$, and drive frequency 40 kHz above $\Omega_0/2\pi$. Flow begins near the separatrix and evolves toward either focus. (b) Experimental phase space mean trajectory from focus 1 to focus 2 (8000 averages). (c) Data for phase space mean trajectory from focus 2 to focus 1 (8000 averages). (d) and (e) Experimental time traces for the two switching transitions (8000 averages).

this classic problem: Here, there is a basin of attraction about each of the two foci found on a Poincaré map of the configuration space. Instead of a one-dimensional potential well, there is a quasipotential, with the dynamics governed by the noise energy at each point in the configuration space[20]. The equivalent activation energy, E_A,

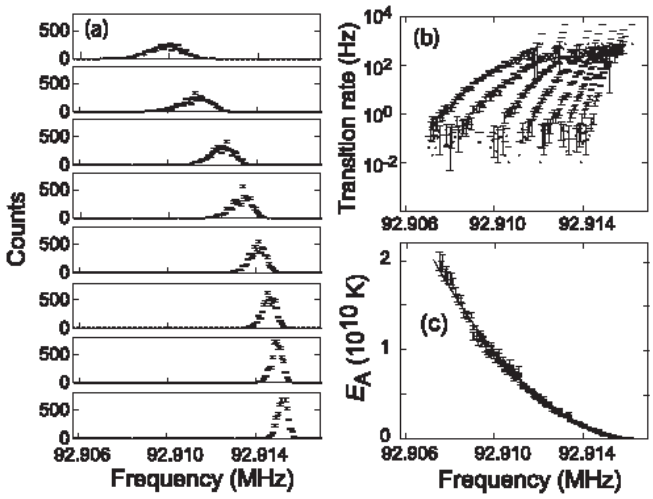

FIG. 3: (a) Switching histograms $h(\nu)$ for different noise powers, with $\mathcal{B}$ =-56 dBm, 5 dB above the critical point, for transitions from focus 1 to 2. (b) Transition rates $\Gamma(\nu)$ extracted from the switching histograms. (c) Calculated energy barrier $E_A(\nu)$ extracted from the transition rates and the variation in noise power. The noise power was varied from -127 dBm/Hz to -113 dBm/Hz.

for transitions between the foci, is found by integrating the minimum available noise energy over the trajectory between the foci.

Transitions were induced by using an external broadband white noise signal, combined with the radiofrequency drive signal using a directional coupler, to generate a signal that included both the drive signal $\mathcal{B}$ and the noise signal $\mathcal{B}_n$. Typical noise powers ranged from -130 to -100 dBm/Hz. The drive signal itself was produced by a source with very low phase noise; with no additional noise power, transitions were still induced by this remnant phase noise, to which the resonator is very sensitive. The thermal noise of the circuit, and the mechanical noise associated with the finite resonator Q, are estimated to be 70 dB below the source phase noise, and were too small to induce measurable transitions in the system.

Transition histograms were measured by applying a drive signal to the resonator above the critical value, preparing the resonator in one of the two basins of attraction, and monitoring the switching transitions to the other basin. We measured histograms of the switching probability per unit time, $h(t)$, by sweeping the drive frequency $\nu(t) = \Omega(t)/2\pi$ at a constant rate $s = d\nu/dt$, and recording the drive frequency at which a transition occurred. This is a technique that has been extensively used for measuring switching distributions in current-biased Josephson junctions[21]. The transition rate $\Gamma(\nu)$ is extracted from the histogram $h(t)$ using $\Gamma(\nu(t)) = (1 - \int_{-\infty}^{t} h(t')dt')^{-1}\, s\, h(t)$.

In Fig. 3(a) we display a set of histograms $h(\nu(t))$; higher noise powers shift the peak switching frequency and also broaden the distribution. In Fig. 3(b) we show the transition rates extracted from these histograms, demonstrating the rapid increase in transition rate as the noise power is increased. We then extract the quasi-activation energy $E_A(\nu)$, by inverting the thermal activation expression $\Gamma(\nu) \equiv \Gamma_0 \exp(-E_A(\nu)/k_B T_{eff})$, where the effective temperature T_{eff} is proportional to the noise power, and the prefactor Γ_0 is related to the Kramers low-dissipation form[19], $\Gamma_0 \approx \nu_0/Q$. We note that in this technique, the histograms are only logarithmically sensitive to Γ_0, so that a precise determination is difficult. In Fig. 3(c) we display the activation energy $E_A(\nu)$ extracted from the histograms, showing the expected decline in the barrier energy as the drive frequency approaches the critical frequency. The distributions shown in Fig. 3(b) are seen to collapse onto a single curve $E_A(\nu)$. In Fig. 4(a) we show a collection of experimentally measured $E_A(\nu)$ curves, measured for transitions from focus 1 to 2 and from 2 to 1, for different drive amplitudes.

We calculated the activation energies numerically. The dynamic solutions to Eq. (1) without noise give the relaxation from the separatrix to one of the foci. During a noise-induced transition, the system is excited from a basin near a focus *towards* the separatrix, which it crosses and then relaxes to the other focus. There is an infinite number of possible trajectories that allow a transition. Given a specific trajectory, it is possible to calculate the contribution of the noise force using Eq. (1). The total energy transferred to the resonator for a particular trajectory is found by integrating the noise power along that trajectory, thus yielding the effective quasienergy between the foci. The energy transferred is thus an action-like quantity, and the most likely escape trajectory is that which requires the minimum action. The action-like integral S of the system is then $S = \int_{path} \mathcal{B}_n^2(t)dt$.

The most likely path $Y_0(t)$ minimizes the integral S. Because the separatrix is a saddle point, the extremal trajectory will most likely travel near the separatrix. The oscillator will naturally evolve from a point near the separatrix to either focus, without contributing to the action-like integral, as this relaxation does not require a noise term. Only when the oscillator is evolving against the dissipative flow field, from a focus toward the separatrix, will it contribute to the action integral.

We used a numerical minimization of the possible trajectories $Y(t)$, using S as a test function to approach the extremum trajectory $Y_0(t)$. Minimum trajectories were calculated for different drive frequencies and amplitudes, yielding the energy barrier as a function of the drive amplitude, shown in Fig. 4(b). We find good agreement (to logarithmic accuracy) between the measured and calculated energy barriers.

Near the critical drive power $\mathcal{B}_c$, analytic forms indicate that the energy barrier should have a quadratic dependence on the offset from the critical frequency $(\nu - \nu_c)^2$ (where $\nu_c = \nu_{U,L}$)[16] . This quadratic dependence is shown in Fig. 3(c) for one drive power, and for a

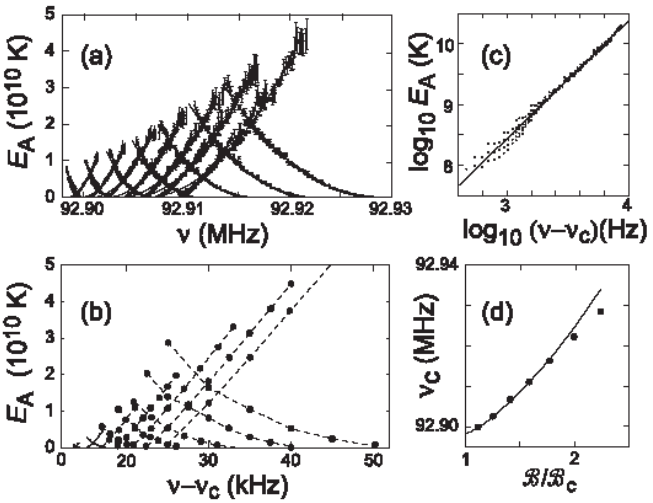

FIG. 4: (a) Measured quasienergy barrier for a drive force ranging from 1 dB to 7 dB above the critical force $\mathcal{B}_c$. (b) Numerically-calculated energy barriers between foci 1 and 2, assuming a Duffing oscillator with the same frequency, quality factor, and nonlinearity as measured from Fig. 1. (c) Log-log plot showing $E_A \propto (\nu - \nu_c)^2$ dependence of the energy barrier near the critical point. (d) ν_c versus drive amplitude $\mathcal{B}/\mathcal{B})c$. At large amplitudes the data diverges from the analytic form.

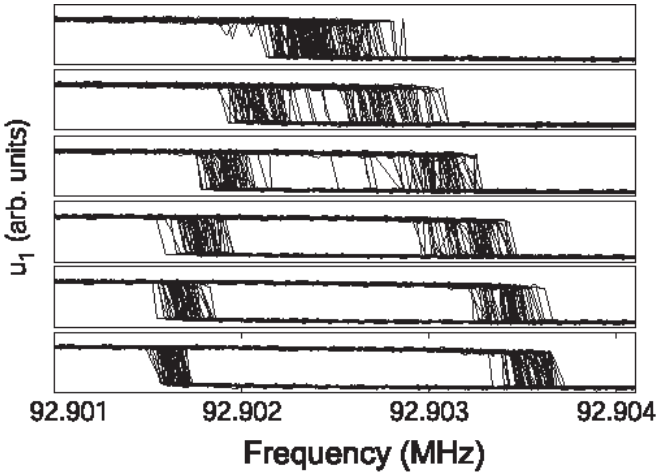

FIG. 5: Amplitude hysteresis plots, for no noise power (bottom), with the drive amplitude set at -59 dBm, 2 dB above the critical point. The noise power was increased in 2 dB steps for each succeeding frame. At the largest noise power, the hysteresis is quenched.

range of different drive powers in Fig. 4(c). This allows a determination of ν_c for a given drive power; our typical histograms yield an uncertainty of $\Delta\nu_c/\nu_c \approx 3 \times 10^{-7}$. By comparing the experimentally-observed dependence of ν_c on drive power with that obtained from numerical analysis of the Duffing equation, shown in Fig. 4(d), we can extract the natural resonance frequency ν_0 and the coefficient of nonlinearity K; the former is the intercept of the curves shown in that figure, and the latter related to the slope of the curves at small drive powers. We find $\nu_0 = 92887360 \pm 10$ Hz and $K = (3745 \pm 4) \times 10^{11}$ N/m^3. The frequency measurement represents a relative precision of $\Delta\nu_0/\nu_0 \approx 1.1 \times 10^{-7}$. This level of frequency resolution has significant implications for e.g. mass sensing with mechanical resonators[2,22].

The measurements described above were made in the small-to-moderate noise limit, with noise energies much less than the energy barrier. At higher noise powers, the hysteresis due to the nonlinear response can actually be quenched, by rapid noise-induced transitions between the two foci. This quenching is demonstrated in Fig. 5: As the noise power is increased, the area of the hysteresis loop grows visibly smaller, until, at the highest noise powers, the switching is no longer hysteretic. In this limit, the oscillator generates random telegraph signals as it makes transitions from one focus to the other. The spectrum of the random telegraph signal is related to the transition rate of the oscillator.

In conclusion, we have measured the configuration space trajectories, and the transition rates, between the bistable states of a nonlinear radiofrequency mechanical resonator. These measurements are in good agreement with numerical simulations based on the Duffing oscillator equation of motion. Detailed analysis of the noise-induced switching transitions allows a quantitative measurements of the energy barrier between the stable foci, and provides a highly sensitive measurement of two key resonator parameters, the resonator natural frequency and the nonlinear parameter.

Acknowledgments. We would like to thank C.S. Yung, R. G. Knobel, D. R. Schmidt, L. J. Swenson, and D. K. Wood for their support. This work was funded by the DARPA-DMEA/UCSB Center for Nanoscale Innovation for Defense.

[1] A. N. Cleland and M. L. Roukes, Appl. Phys. Lett. **69**, 2653 (1996).
[2] K. L. Ekinci, X. M. H. Huang, and M. L. Roukes, Appl. Phys. Lett. **84**, 4469 (2004).
[3] B. Ilic, D. Czaplewski, H. G. Craighead, P. Neuzil, C. Campagnolo, and C. Batt, Appl. Phys. Lett. **77**, 450 (2000).
[4] D. S. Greywall, B. Yurke, P. A. Busch, A. N. Pargellis, and R. A. Willett, Phys. Rev. Lett. **72**, 2992 (1994).
[5] D. W. Carr, S. Evoy, L. Sekaric, H. G. Craighead, and J. M. Parpia, Appl. Phys. Lett. **75**, 920 (1999).
[6] A. N. Cleland and M. L. Roukes, J. Appl. Phys. **92**, 2758 (2002).
[7] R. G. Knobel and A. N. Cleland, Nature **424**, 291 (2003).
[8] A. D. Armour, M. P. Blencowe, and K. C. Schwab, Phys. Rev. Lett. **88**, 148301 (2002).
[9] K. L. Ekinci, Y. T. Yang, and M. L. Roukes, J. Appl. Phys. **95**, 2682 (2004).
[10] S. M. Carr, W. E. Lawrence, and M. N. Wybourne, Phys. Rev. B **64**, 220101/1 (2001).
[11] K. L. Turner, S. A. Miller, P. G. Hartwell, N. C. MacDonald, S. H. Strogartz, and S. G. Adams, Nature **396**, 149 (1998).
[12] W. Zhang, R. Baskaran, and K. L. Turner, Sensors and Actuators A **102**, 139 (2002).
[13] S. M. Soskin, R. Mannella, and P. V. E. McClintock, Phys. Rep. **373**, 247 (2003).
[14] B. Yurke, D. S. Greywall, A. N. Pargellis, and P. A. Busch, Phys. Rev. A **51**, 4211 (1995).
[15] A. H. Nayfeh, *Nonlinear oscillations* (Wiley, New York, 1979).
[16] M. Dykman and M. Krivoglaz, Sov. Phys. JETP **50(1)**, 30 (1979).
[17] A. N. Cleland, M. Pophristic, and I. Ferguson, Appl. Phys. Lett. **79**, 2070 (2001).
[18] K. L. Ekinci, Y. T. Yang, X. M. H. Huang, and M. L. Roukes, Appl. Phys. Lett. **81**, 2253 (2002).
[19] H. A. Kramers, Physica **7**, 284 (1940).
[20] R. L. Kautz, Phys. Lett. A **125**, 315 (1987).
[21] T. A. Fulton and L. N. Dunkleberger, Phys. Rev. B **9**, 4760 (1974).
[22] B. Ilic, H. G. Craighead, S. Krylov, W. Senaratne, C. Ober, and P. Neuzil, J. Appl. Phys. **95**, 3694 (2004).